NJC

PAPER

View Article Online
View Journal | View Issue



Cite this: *New J. Chem.*, 2015, 39, 2146

# A tough, smart elastomeric bio-based hyperbranched polyurethane nanocomposite

Suman Thakur and Niranjan Karak*

Received (in Montpellier, France) 8th November 2014,
Accepted 2nd January 2015

DOI: 10.1039/c4nj01989j

www.rsc.org/njc

Herein, we fabricate an elastomeric nanocomposite using castor oil-based hyperbranched polyurethane (HPU) and iron oxide nanoparticles decorated reduced graphene oxide (IO–RGO) nanohybrid by an *in situ* polymerization technique. The designed nanocomposite not only exhibits good thermal properties but also possesses excellent mechanical properties such as tensile strength (24.15 MPa), tensile modulus (28.55 MPa) and toughness (110.8 MJ $m^{-3}$). In addition, the nanocomposite demonstrates rapid and repeatable self-healing abilities under exposure of 20–30 s microwave power input (180–360 W) and by direct sunlight exposure ($10^5$ lux) for 5–7.5 min. It also demonstrates excellent shape-recovery ability under microwave power (30–60 s) as well as in direct sunlight (1–2.5 min). Thus, the studied tough polymeric material has potential advanced applications.

## Introduction

Smart materials with a response to a stimulus are attracting significant interest in the material science field due to their diverse potential applications. Among these, self-healing and shape-memory materials are attracting the most attention from material scientists. The self-healing ability is a crucial feature of biomaterials, and increases the durability of natural materials,[1] whereas man-made materials are susceptible to failure upon encountering damage or fracture by external factors during their service life. Thus, the development of self-healing materials which can repair themselves after mechanical damage has been highly desired over the past decade.[2–4] A variety of methods have been developed to access such materials, in particular, the employment of self-healing polymers (SHPs). In most of the approaches to date, micro-capsules containing healing agents are embedded in the polymeric matrix to achieve such properties.[5,6] In these cases, the healing agent is released, owing to a capillary effect, into cracks to repair them. These types of SHPs can heal themselves spontaneously, as and when required. But they can be healed only once at the same location, due to exhaustion of the healing agent from the containers. To overcome this short-coming, material scientists designed a three-dimensional micro-vascular network with a suitable healing agent, as well as a ''reversible polymer'' which contains reversible bonds such as non-covalent or dynamic covalent bonds.[7–9] This type of healing system can be used to heal the cracked site of the material repeatedly. As the healing agents are delivered to the crack site by the three-dimensional micro-vascular network, it can be healed repeatedly, even at the same location. On the other hand, the reversible bonds are able to reversibly associate and dissociate during triggering from an external stimulus, such as heat or light.[10] They tend to open immediately upon damage on exposure to a stimulus, due to the presence of such weak bonds. These dynamic bonds repair the fractured/damaged areas by driving the polymer chains to the site through diffusion and re-entanglement above the glass transition temperature. Despite their great advances, some serious problems limit their practical applicability. Both three-dimensional micro-vascular network embedded self-healing materials and reversible polymers suffer from poor mechanical properties, along with high costs.[11,12]

Thus, the development of a novel SHP with repeated healing efficiency and outstanding mechanical properties is still a key challenge. To address this problem, Huang and co-workers designed a polyurethane–graphene nanocomposite as a self-healing material.[13] These nanocomposites demonstrated repeated healing efficiency by infrared (IR) light, electricity and microwave (MW) energy with good mechanical properties. However, to achieve such healing properties, the amount of graphene, as well as the MW power consumption, is quite high. Thus, the use of such stimuli is difficult in practical field applications. Thus, emerging materials with a rapid and repeatable self-healing capability with adequate mechanical properties still remain a daunting challenge.

Recently, a new concept has been explored on the use of shape-memory materials, such as shape-memory alloy (SMA)-based wires and shape-memory polymer (SMP)-based fibers to improve the self-healing process by providing a mechanism to repair the crack, either partially or fully.[14,15] This can also offer

*Advanced Polymer and Nanomaterial Laboratory, Centre for Polymer Science and Technology, Department of Chemical Sciences, Tezpur University, Tezpur 784028, India. E-mail: karakniranjan@gmail.com; Fax: +91-3712-267006; Tel: +91-3712-267327*

 

a repeated healing capability with improved mechanical properties. But it also suffers from some inadequacies. For instance, in order to achieve effective healing, SMA wires or SMP fibers have to be positioned locally and perpendicular to the crack.[16] This is indeed a challenge to achieve in practical applications. Thus, an SMP without any external shape-memory material has an immense potential to overcome the above-mentioned shortcoming. In this context, Rowan *et al.* designed a semicrystalline polydisulfide network, which inherently exhibited both shape-memory and healable properties.[17] This polydisulfide network demonstrated thermo shape-memory and photohealable properties. Also, Zhao and co-workers fabricated polyethylene–carbon black nanocomposites, which showed improved self-healing by a shape-memory effect.[18] However, these materials did not show multistimuli responsive behavior.

In the current scenario, hyperbranched polyurethanes (HPU)–reduced graphene oxide (RGO) nanocomposite exhibited multistimuli responsive shape-memory behavior under MW, sunlight and thermal energy.[19] In addition, the use of iron oxide–RGO (IO–RGO) nanohybrids instead of RGO only had some advantages, as IO nanoparticles have good thermal conductivity, magnetic behavior and MW absorbing capacity. Also, RGO contains some functional groups on its surface, so dispersion into the polymer matrix is easy.[20,21] Here, it is pertinent to mention that self-healing by a natural stimulus like sunlight is an eco-friendly, inexpensive, and practical strategy, and hence more promising. Ghosh and Urban developed a polyurethane based on an oxetane-substituted derivative of chitosan, which could mend itself under exposure to sunlight.[8] Most importantly, RGO also has an excellent sunlight absorbing capacity like graphene and, hence, it can be used for this purpose.[22] Furthermore, IO nanoparticles are well-known for their good microwave absorbing capacity, excellent thermal conductivity, high magnetic saturation value, *etc.*[23] Therefore, IO–RGO nanohybrids can be used to enjoy their combined effects.

Herein, a tough self-healing elastomeric nanocomposite of an HPU and IO–RGO nanohybrid was fabricated. Evaluations of the mechanical properties, multi-stimuli self-healing and shape-memory behavior of the nanocomposite by sunlight and microwave were performed.

# Experimental

## Materials

Castor oil (Sigma Aldrich), 1,4-butanediol (BD, Merck, Germany), and poly(ε-caprolactone) diol (PCL, $M_n$ = 3000 g mol$^{-1}$), (Solvay Co., UK) were used after drying in an oven prior to use. Ferrous chloride (Merck, India), anhydrate ferric chloride (Merck, India), and 2,4/2,6-toluene diisocyanate (TDI, Merck, Germany) were used as received. Xylene (Merck, India) and *N*,*N*-dimethylacetamide (Merck, India) were vacuum-distilled and kept in a 4A type molecular sieve before use. Other chemicals and solvents were used without further purification. Graphene oxide (GO) was prepared by a modified Hummers method. The oxidization of graphite powder was achieved using a mixture of concentrated sulphuric acid and $KMnO_4$, as reported in our earlier work.[20] The monoglyceride of the castor oil was prepared as reported earlier.[24]

## Preparation of iron oxide–reduced graphene oxide (IO–RGO) nanohybrid

The nanohybrid was prepared by the co-precipitation of ferrous and ferric ions on the GO sheets, followed by the reduction of GO, as reported in our earlier work.[25] Briefly, 64.8 mg of $FeCl_3$ and 39.6 mg of $FeCl_2$ were mixed with 50 mL of GO dispersion in millipore water (1 mg mL$^{-1}$). Then, the mixture was stirred constantly for 1 h under a $N_2$ atmosphere. Then, 20 mL of banana peel ash extract and 10 mL of *Colocasia esculenta* leaf extract were added and stirred for 30 min to obtain the IO–RGO nanoparticles-based nanohybrid. The ratio of iron oxide and reduced graphene oxide in the nanohybrid was 1 : 1 in the prepared nanohybrid.

## Preparation of hyperbranched polyurethane iron oxide–reduced graphene oxide (HPU–IO–RGO) nanocomposite

A three-neck round-bottomed flask equipped with a nitrogen gas inlet, a mechanical stirrer, and a Teflon septum was used for the nanocomposite preparation. The required amounts of PCL (0.002 mol), BD (0.004 mol), and dispersed IO–RGO nanohybrid (in DMAc) were added to the round bottomed flask containing the desired amount of xylene with constant stirring (37% solid content). After dissolving PCL, the desired amount of TDI (0.007 mol) was added dropwise, using a syringe, into the reaction mixture at room temperature. The reaction was continued for 3 h at a temperature of 70 ± 2 °C to obtain the desired viscous mass, which was treated as the pre-polymer.

This pre-polymer was then cooled to room temperature and the monoglyceride of castor oil (0.002 mol) as a triol was added with the required amount of TDI (0.002 mol) to maintain the overall NCO/OH ratio equal to one. The temperature was then raised to 110 ± 2 °C and stirred continuously for 2.5 h to complete the reaction, as indicated by the absence of an isocyanate band at 2270 cm$^{-1}$ in the FTIR spectrum. Hyperbranched polyurethane was also prepared without the IO–RGO nanohybrid. Hyperbranched polyurethane nanocomposites with 0.5 weight%, 1 weight%, and 2 weight% of IO–RGO nanohybrid were encoded as HPU–IO–RGO0.5, HPU–IO–RGO1, and HPU–IO–RGO2, respectively, and hyperbranched polyurethane without IO–RGO nanohybrid was coded as HPU.

## Instruments and testing methods

The tensile strength and elongation at break were measured by the help of a Universal Testing Machine (UTM) (Jinan WDW 10, Republic of China) with a 500 N load cell and a cross-head speed of 20 mm min$^{-1}$. The differential scanning calorimetry (DSC) study was done using a DSC 6000 (Perkin Elmer, USA) at a heating rate of 2 °C min$^{-1}$ under a nitrogen flow of 30 mL min$^{-1}$ from −20 °C to 120 °C. TGA was done using a thermal analyzer, TGA 4000 (Perkin Elmer, USA) with a nitrogen flow of 30 mL min$^{-1}$ at heating rate of 10 °C min$^{-1}$.

In order to evaluate the healing performance, films with a thickness of 0.5 mm of the nanocomposite were cut (10 mm$^3$ × 0.2 mm$^3$ × 0.015 mm$^3$ in dimension) in a transverse direction

by a razor blade, and the cracked was healed by sunlight or microwave, separately. The healing efficiency was calculated as the ratio of the tensile strength values of the nanocomposites before and after healing. The tensile strengths of the pristine and the healed samples were measured by the same UTM. Samples were cut into strips of 80 $mm^3 \times 10$ $mm^3 \times 0.50$ $mm^3$ for testing. The tensile strengths of pristine HPU, as well as the nanocomposites with different loadings of the nanohybrid, were measured for at least five samples in each case, before and after the healing process. The optimal healing time for each case was defined as the shortest time required to achieve the best healing efficiency under the given conditions. For MW healing, a domestic microwave oven (800 W) operating at a frequency of 2.45 GHz was used. Three different MW powers (180 W, 360 W, and 540 W) were used for the healing. Sunlight healing was performed under direct sunlight (11 $am^{-2}$ pm) at Tezpur University campus (altitude: 26.63°N 92.8°E) in the month of November on sunny days [average temperature (29 ± 1 °C) and humidity (65 ± 1%)], with a light intensity of 90 000–100 000 lux.

To study the shape-memory behavior under MW and direct sunlight, bending tests were performed. The sample was folded in a ring form at 60 °C, followed by quenching into an ice-salt bath for 5 min at −10 °C. Then the shape recovery of the nanocomposite films was achieved by exposure to MW irradiation of 360 W for 30–60 s under ambient conditions or in direct sunlight on sunny days in November, 2013. The shape recovery was calculated using the following equation.

$$\text{Shape recovery (\%)} = \{(90 - \theta)/90\} \times 100 \qquad (1)$$

where $\theta$ in degrees denotes the angle between the tangential line at the midpoint of the sample and the line connecting the midpoint and the end of the curved sample.

## Results and discussion

### Preparation of the nanocomposite

An *in situ* polymerization technique was used to prepare the HPU–IO–RGO nanocomposite by using the monoglyceride of castor oil as a branch generating moiety and IO–RGO as the reinforcing nanomaterial, as shown in Scheme 1. It is pertinent to mention here that the average functionality of castor oil is about 2.7, but the monoglyceride of it contains a small amount of unreacted glycerol, castor oil and diglyceride. Thus, the average functionality of the monoglyceride is taken as 3 for simplicity.

The crucial monitoring factors during nanocomposite preparation are the concentration of the reactants (especially the multifunctional moiety), the addition rate of the multifunctional moiety, reaction time, and temperature.[26] During the nanocomposite preparation, the dispersion of the IO–RGO nanohybrid in DMAc was incorporated in the 1st step of the polymerization to obtain a strong interfacial interaction (covalent and noncovalent) with HPU chains. In the 2nd step of the reaction, the multifunctional moiety was slowly added in a very dilute solution (15% in xylene) to avoid gel formation, and also temperature of the reaction was gradually raised to 110 °C.[26]

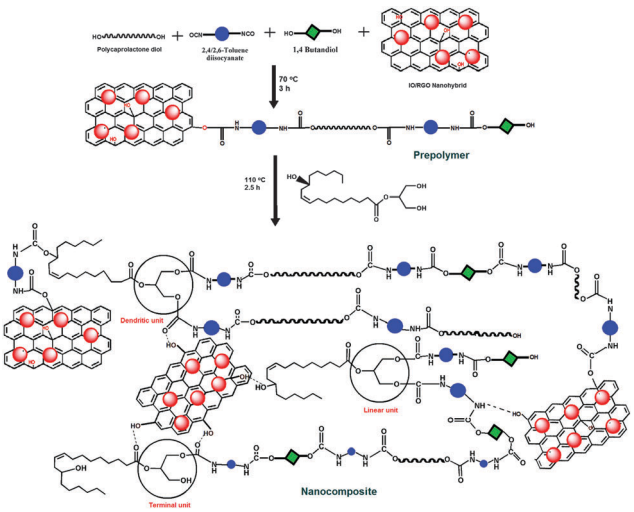


Scheme 1 Synthesis of HPU–IO–RGO nanocomposite.

### Characterization of the nanocomposite

FTIR spectra confirmed the presence of urethane linkages, both in HPU and its nanocomposites (see Fig. 1). In the studied HPU and its nanocomposites, the appeared vibration bands at 1680–1695 $cm^{-1}$ were attributed to a C=O stretching vibration (contribution from both amide I and ester linkage). Furthermore, N–H stretching and N–H bending vibrations were observed at 3430 $cm^{-1}$ and 1557–1580 $cm^{-1}$, respectively. A few more characteristic bands for the urethane linkage were found at 1060–1090 $cm^{-1}$ (N–H deformation vibration), 1140–1175 $cm^{-1}$ (C–O stretching vibration), *etc.*[24,26] The shifting of the C=O

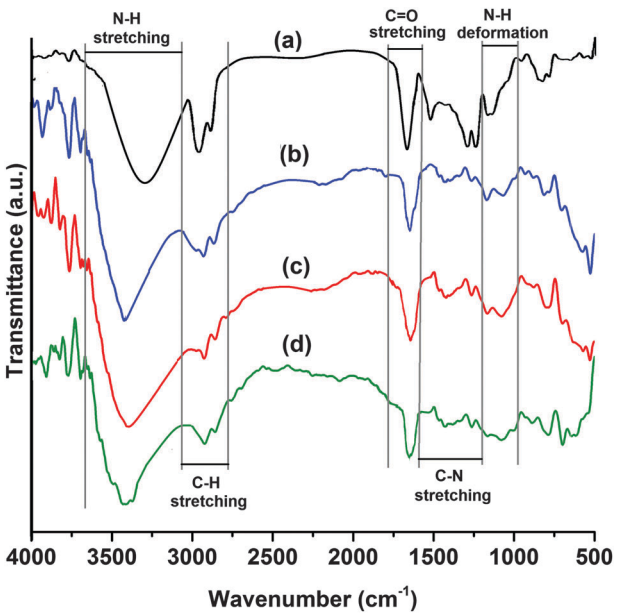


Fig. 1 FTIR spectra of (a) HPU, (b) HPU–IO–RGO0.5, (c) HPU–IO–RGO1 and (d) HPUIO–RGO2.

 

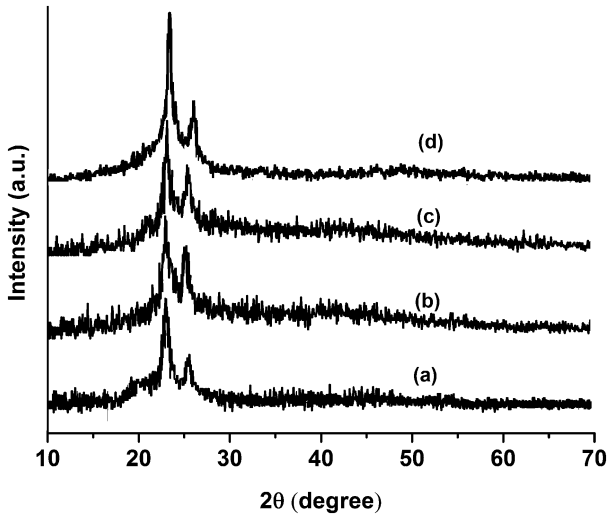


Fig. 2 XRD patterns of (a) HPU, (b) HPU–IO–RGO0.5, (c) HPU–IO–RGO1 and (d) HPU–IO–RGO2.

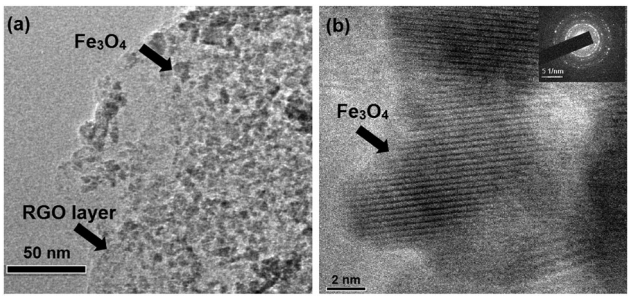


Fig. 3 HRTEM images of HPU–IO–RGO2: (a) at low resolution showing RGO layer and decorated IO nanoparticle and (b) at high resolution showing an individual IO nanoparticle on a RGO sheet (inset shows SAED patterns).

band to 1680 $cm^{-1}$ from 1695 $cm^{-1}$ was observed with the increasing amount of IO–RGO in the nanocomposite.[26] This indicates the presence of interactions among the polymer chains and the IO–RGO nanohybrid. These interactions increase with the increase in the IO–RGO content.

In the XRD patterns, HPU and its nanocomposite exhibited two distinct peaks at $2\theta = 21.15^\circ$ (corresponding to a *d*-spacing of 0.41 nm) and $23.5^\circ$ (corresponding to a *d*-spacing of 0.375 nm), which are attributed to the crystals of the PCL moiety present in HPU (see Fig. 2).[26] After incorporation of the nanohybrid, a slight shifting of the PCL peaks towards a higher angle was observed, which may be due to formation of a more dense structure compared to the pristine HPU.[26] Also the peak intensity of the PCL moiety was slightly increased with the nanohybrid loading.

This indicates that the crystallinity of the nanocomposite increased with the increase dose of nanohybrid, as the nanohybrid acts as a nucleating agent. Here, it is pertinent to mention that no such distinct peak is observed for IO–RGO in the XRD patterns of the nanocomposites. This may be due to the presence of a small amount of IO–RGO in the nanocomposite.

The performance of the nanocomposites is strongly influenced by the dispersion of the nanohybrid in the HPU matrix. Therefore, HRTEM was employed to investigate the dispersion of the nanohybrid. HRTEM images of HPU–IO–RGO2 are shown in Fig. 3. From the figure, it is clear that the nanohybrid is finely distributed in the HPU matrix.

## Mechanical properties

The pristine HPU possesses a low tensile strength and modulus, due to the presence of a hyperbranched structure and the monoglyceride of castor oil in the polymer chains. After incorporation of the IO–RGO nanohybrid, all the nanocomposites exhibited excellent dose-dependent mechanical properties, like tensile strength, tensile modulus and toughness (see Table 1). One noticeable achievement of this study is the simultaneous improvement of tensile strength and elongation at break, which resulted in a high toughness for the nanocomposite. Such outstanding mechanical properties can definitely be attributed to the strong interfacial adhesion and good compatibility between HPU and the nanohybrid.[26,27] Also, the remaining hydroxyl groups in the nanohybrid may react with an isocyanate-terminated prepolymer chain to form a urethane linkage between HPU and the nanohybrid.[21] These strong chemical bonds help to achieve a successful transfer of the load from HPU to the nanohybrid in the nanocomposite.[26] Due to the presence of the afore-stated covalent bonding, H-bonding, and polar–polar interaction between the nanohybrid and the HPU chains, the hard domain of HPU is stiffened. This consequently enhances the tensile modulus of the nanocomposite. The nanocomposite also demonstrated a high dose-dependent toughness after incorporation of the nanohybrid. These nanocomposites also exhibited excellent flexibility with very high elongation at break.

More interestingly, the elongation at the break of the nanocomposites increased with increases in the content of nanohybrid. Such an enhancement was mooted as being due to the alignment of HPU chains in the initial stage of tensile loading, which forces them to orient the nanohybrid along the loading direction. This was also observed in other reported

Table 1 Mechanical properties of the nanocomposites

| Properties | HPU[a] | HPU–IO–RGO0.5 | HPU–IO–RGO1 | HPU–IO–RGO2 | HPU–RGO2[b] |
|---|---|---|---|---|---|
| Tensile strength (MPa) | 7.3 ± 0.7 | 17.15 ± 1.7 | 21.34 ± 2.1 | 24.15 ± 2.3 | 28.3 ± 1.9 |
| Tensile modulus (MPa) | 3.5 ± 0.5 | 10.49 ± 0.4 | 18.5 ± 0.9 | 28.55 ± 1.2 | 37.3 ± 3.2 |
| Toughness (MJ $m^{-3}$) | 26.30 ± 2.8 | 41.8 ± 5.4 | 66.4 ± 6.1 | 110.8 ± 5.4 | 121.78 ± 4.1 |
| Elongation at break (%) | 660 ± 25 | 745 ± 15 | 936 ± 35 | 1090 ± 50 | 1180 ± 34 |

[a] Reproduced with permission.[24] [b] Reproduced with permission.[30]

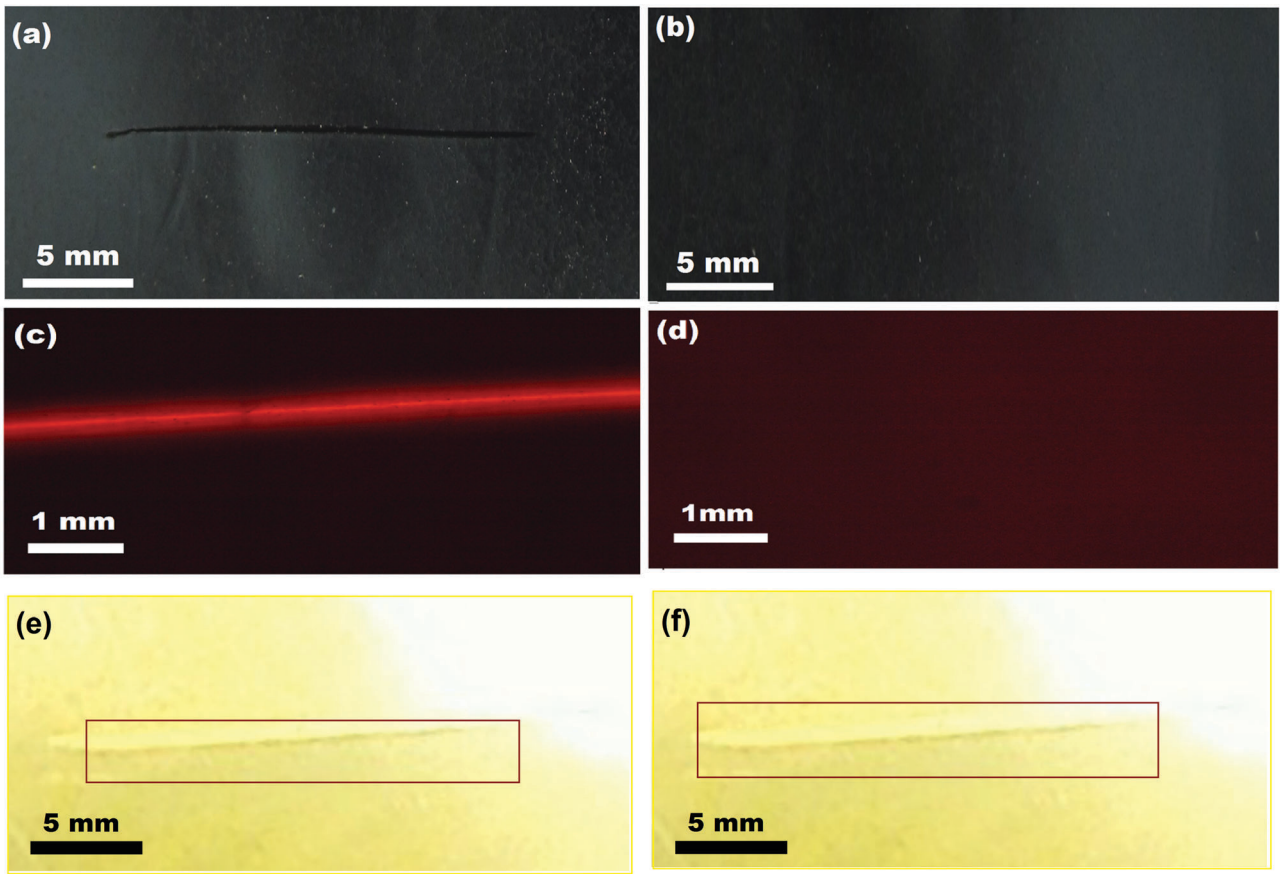


Fig. 4 Digital images of (a) fractured nanocomposite film and (b) healed nanocomposite film, and optical microscopic images of (c) fractured nanocomposite film and (d) healed nanocomposite film, and digital image of HPU (e) before and (f) after healing.

graphene-based polymer nanocomposites.[28,29] Again, at high stress, the layer of RGO in the nanohybrid may slide over each other.[30] From Table 1, a slight deterioration of the mechanical properties of the HPU–IO–RGO nanocomposite is observed from the HPU–RGO nanocomposite. This may be due to the presence of a high aspect ratio of nanomaterial, especially RGO that provides for a mechanically strong nanocomposite.[30] On the other hand, only the IO-based HPU nanocomposite exhibited inferior mechanical properties compared to the HPU–RGO nanocomposite.[31] Therefore, an equal amount of RGO and IO nanoparticle containing nanohybrid was used to fabricate the nanocomposite in this study.

### Self-healing behavior of the nanocomposite

Optical images were used to examine the healing ability of the nanocomposites. The typical optical images for the flaw film before and after healing are shown in Fig. 4. A comparison of the two optical images before and after the healing clearly demonstrate the completion of the healing process of the nanocomposite film. All the nanocomposites were healed rapidly with excellent healing ability after the incorporation of a small amount (0.5–2 weight%) of IO–RGO nanohybrid. On the contrary, the pristine HPU film does not heal, or only partially healed, even after long time exposure to any tested stimulus. The incorporation of the nanohybrid remarkably enhanced the healing abilities of HPU, as clearly reflected by this result. The intrinsic properties of IO–RGO, such as excellent MW absorbing capacity and high thermal conductivity, as mentioned earlier, are responsible for this observation.[21]

The healing efficiencies of the nanocomposite films under MW are shown in Fig. 5. This shows that the nanocomposite films were healed with a high healing efficiency of 99% or more. The healing efficiency of the nanocomposite by MW depends on the amount of nanomaterial, the MW power input, and the exposure time (see Fig. 5a–c). An increase in any of these parameters results in improvements in the healing efficiency. Here, it is pertinent to mention that pristine HPU only slightly healed (10–15%) after 5 min of MW exposure. Although the HPU–RGO2 nanocomposite was completely healed within 4 min at a high MW power input of 540 W. The healing of HPU–IO–RGO nanocomposites was faster due to the presence of a high amount of iron oxide in the nanohybrid (an equal amount to RGO), which have high MW absorption capacity,[21] and therefore, the nanohybrid absorbs sufficient energy to heal the cracked rapidly.

All the nanocomposites were rapidly healed within 20–30 s under low MW power (360 W only). During the healing process, the nanohybrid works as a nanoscale heater, as well as a heat carrier unit. The nanohybrid absorbed MW energy and started to oscillate its dipoles, the friction from which generated heat at the nanohybrid–polymer interface.[31] This energy was efficiently

 

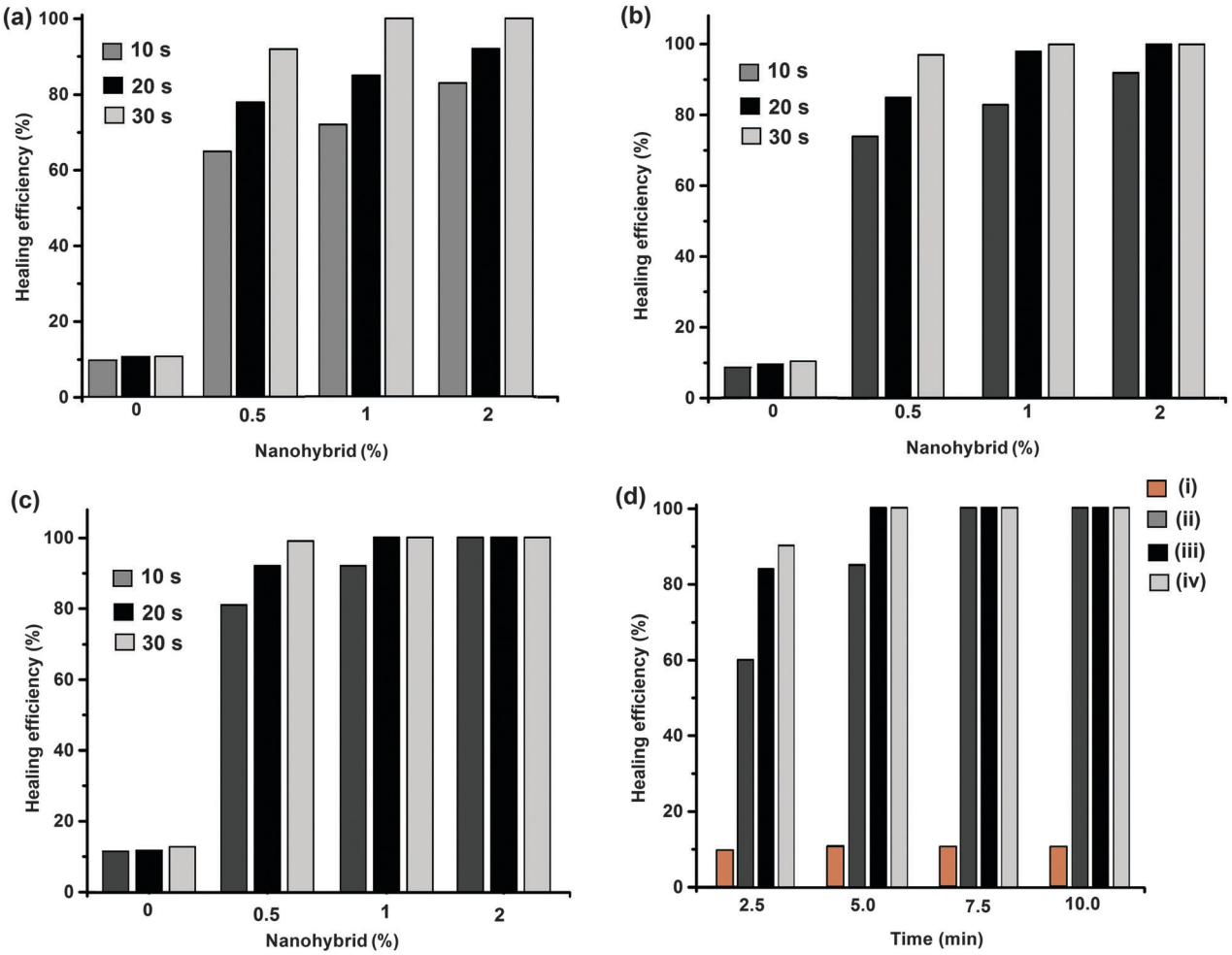


Fig. 5 The healing efficiency at MW power of (a) 180 W, (b) 360 W and (c) 540 W, and (d) under direct sunlight for different loadings of nanohybrid (i) 0%, (ii) 0.5%, (iii) 1% and (iv) 2%.

transferred to the HPU matrix by the nanohybrid, which aids the rapid Brownian movements of the soft segment of the nanocomposite to above the transition temperature (*i.e.*, the melting temperature of the soft segment of HPU (see Fig. 6). These Brownian movements of the HPU chains increase with nanohybrid loading. Hence, the nanocomposite films were heated uniformly and rapidly upon exposure to a stimulus. This helps to permanently repair the flaw, as diffusion occurs at that flaw site, and also, the process can be repeated multiple times. The HPU–IO–RGO2 nanocomposite demonstrated faster healing compared to the other studied nanocomposites, although it had more molecular restriction. This is due to the presence of a higher amount of nanohybrid in it, which helps to absorb more MW energy and helps to transfer this energy to the HPU matrix for rapid healing. As self-healing was achieved by the rearrangement and diffusion of the soft segments of HPU, the healing of the prepared nanocomposite could be repeated again and again.[32] As a result, even after the fifth cycle of the experiment, the healing ability of the nanocomposite remains almost the same (see Fig. 7).

The nanocomposite with 1% and 2% of nanohybrid demonstrated rapid healing within 5 min, with excellent healing efficiency under direct sunlight exposure (see Fig. 5d). But the nanocomposite with 0.5% IO–RGO could only be healed after 7.5 min. These results indicate dose-dependent healing, as well as that this loading of nanohybrid is sufficient for the healing process under sunlight. Similar to MW, the light energy is efficiently transferred throughout the nanocomposite and aids the rapid Brownian movement of the molecular chains of the segment. This causes the rapid healing of the nanocomposite, as diffusion of the chains at the flaw site takes place easily. Here, also the nanocomposite was repeatedly healed by sunlight, and even after the fifth cycle of the experiment, no significant decrease in efficiency was observed (see Fig. 7).

The study also revealed that the used energy of the stimulus was inadequate to cause any degradation or dimensional instability, as confirmed by the thermal study of the nanocomposites.

## Thermal properties

Fig. 8a demonstrated that the melting point ($T_m$) of the soft segment (PCL moiety) increases from 48.2 °C to 52.4 °C upon the incorporation of 2 wt% nanohybrid in the HPU matrix. The presence of the nanohybrid may restrict the molecular motion of the polymeric chains in the initial stages.[26] This may be the reason for the increment of $T_m$. Also, this influence depends on the interaction of the nanohybrid with the HPU chains.

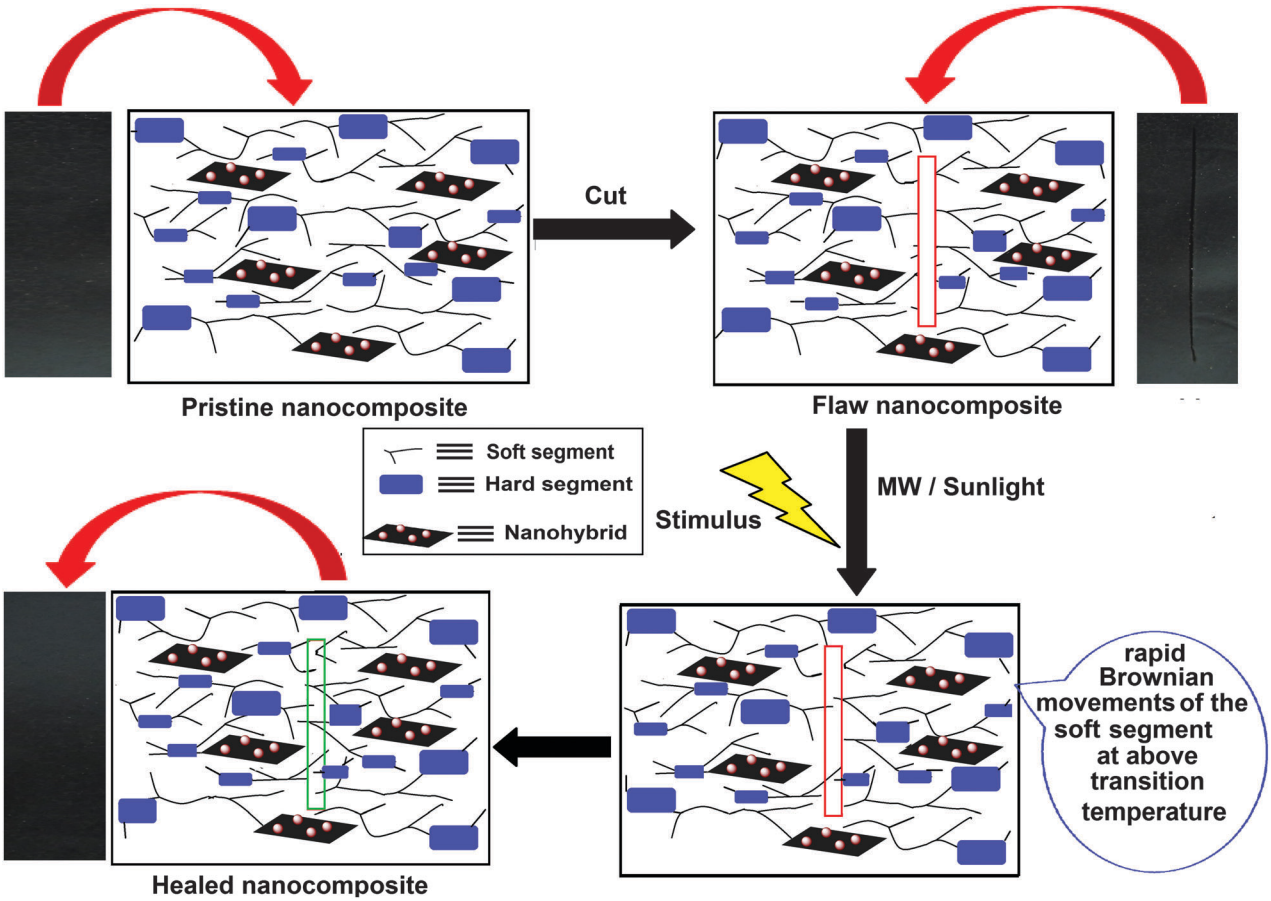


Fig. 6 Plausible healing mechanism of the nanocomposite.

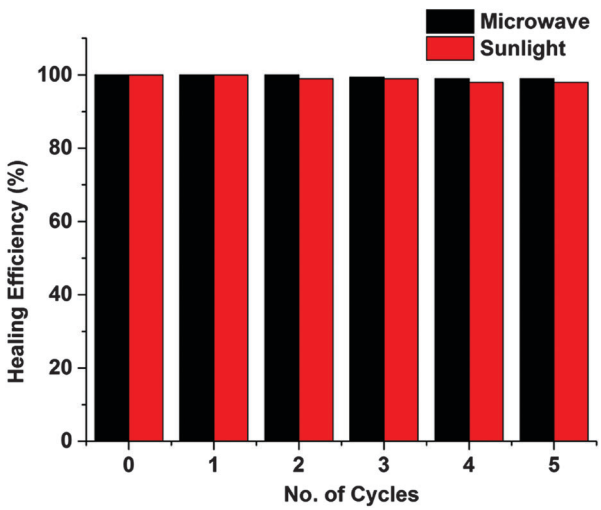


Fig. 7 Healing efficiency of HPU–IO–RGO2 nanocomposite for repeated cycles under MW (at 360 W) and sunlight stimuli.

This clearly suggests that IO–RGO acts as a nucleating agent in the matrix, and thus the presence of the nanohybrid can improve the crystallization process by bringing about the arrangement of the HPU chains in a particular way.[33]

Thermogravimetric analysis (TGA) was performed to verify the thermal stability of the HPU and its nanocomposite (see Fig. 8b). All the thermograms showed two-step degradation patterns. The degradation temperatures of the nanocomposites were enhanced compared to HPU. This suggests the good dispersibility of IO–RGO in the HPU matrix. The improved thermo-stability of the nanocomposites with the loading of the nanohybrid is due to the limited motion of the HPU chains, due to the presence of different physico-chemical interactions.[34] The produced volatiles during the decomposition were also retained for a longer time in the matrix, due to the better barrier characteristic compared to the pristine HPU.[35]

### Shape-memory behavior of the nanocomposite

Furthermore, all the nanocomposites exhibited multi-stimuli responsive shape-memory behaviors. Shape-memory behaviors of the nanocomposite by MW are shown in Fig. 9. Shape-memory tests were also performed under the exposure of MW and sunlight. The shape-recovery time and ratio under different stimuli are tabulated in Table 2. In all cases, the shape-recovery time decreased with the increase of nanohybrid content in the nanocomposites.

The nanohybrid created a large amount of stored elastic strain energy, due to the strong interfacial interactions with the compatible HPU matrix.[26] This assisted the nanocomposites to

 

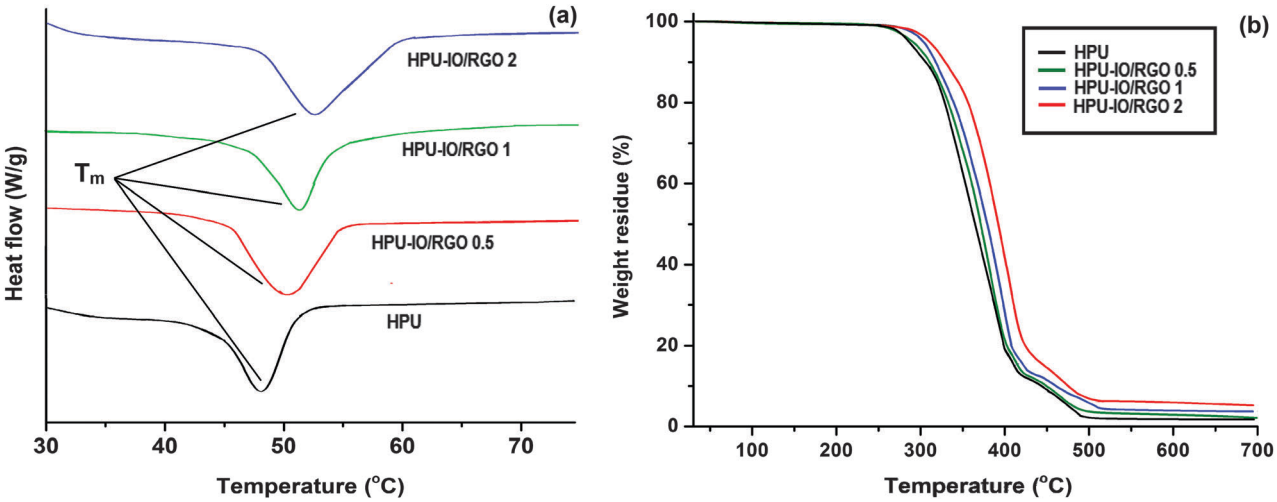


Fig. 8 (a) DSC curve showing the melting temperature of the soft segment of HPU and its nanocomposites and (b) TGA thermograms of HPU and its nanocomposites.

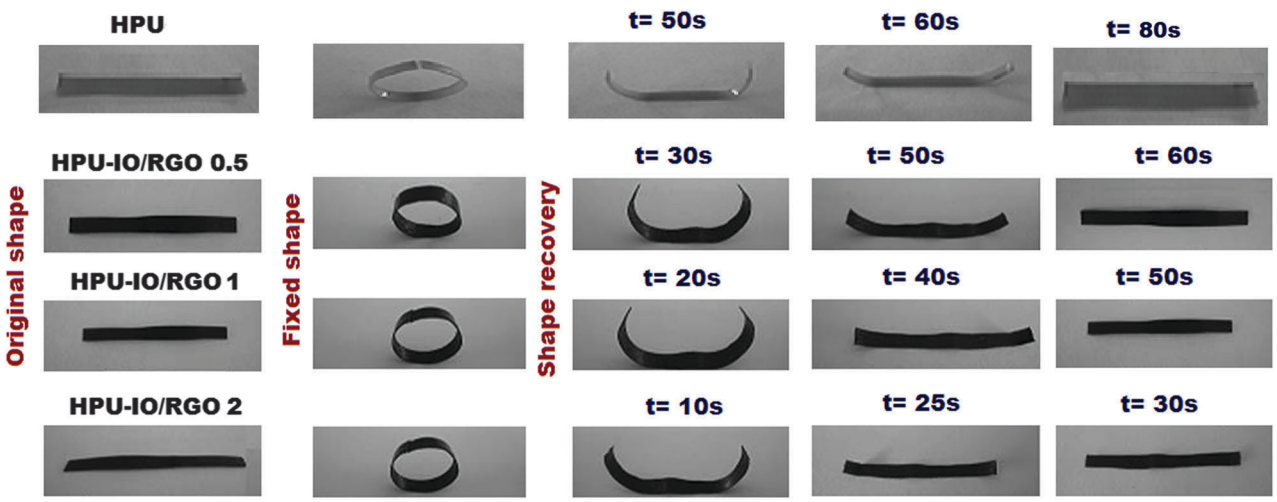


Fig. 9 Shape memory behavior of the nanocomposites under MW stimulus.

Table 2 Shape memory properties of the nanocomposites

| Stimulus | | HPU | HPU–IO–RGO0.5 | HPU–IO–RGO1 | HPU–IO–RGO2 | HPU–RGO2 |
|---|---|---|---|---|---|---|
| MW | Shape recovery time (s) | 80 | 60 | 50 | 30 | 53 |
| | Shape recovery (%) | 95.5 | 96.4 | 97.4 | 99 | 97.6 |
| Sunlight | Shape recovery time (min) | 7 | 2.5 | 2 | 1 | 1.5 |
| | Shape recovery (%) | 95.3 | 96.1 | 97.2 | 98.5 | 98.1 |

achieve a high recovery speed due to the release of this stored elastic strain. Also, the enhancement of the MW and sunlight absorbing capacity with the increase of the nanohybrid content is another important factor for fast recovery.

## Conclusions

In summary, we demonstrated a self-healable and shape-recoverable hyperbranched polyurethane nanocomposite with outstanding mechanical properties. The obtained nanocomposites exhibited a repeatable and rapid healing ability under different stimuli, namely, microwave and sunlight, as well as excellent shape-memory behavior under the same stimuli. In contrast to the existing reported self-healing systems, these nanocomposites showed rapid and repeatable healing ability under green stimuli, particularly under sunlight, which is eco-friendly, inexpensive and practically useful. A few more stimuli, such as magnetic, electric and infrared light, may also be used for the same purpose. The nanocomposite has potential

applications in transport, construction, electronics and more such industries.

## Acknowledgements

S.T. sincerely acknowledges the receipt of his Senior Research Fellowship from the Council of Scientific and Industrial Research (CSIR), India. The authors also express their gratitude to FIST program-2009 (DST), India through the grant No. SR/FST/CSI-203/209/1 dated 06.05.2010. The research is funded by Department of Science and Technology (DST), India through the grant No. SR/S3/ME/0020/2009-SERC, dated 9th July, 2010.

## Notes and references

1 R. J. Varley, D. A. Craze, A. P. Mouritz and C. H. Wang, *Macromol. Mater. Eng.*, 2013, **298**, 1232–1242.
2 R. P. Wool, *Soft Matter*, 2008, **4**, 400–418.
3 B. C. Tee, C. Wang, R. Allen and Z. Bao, *Nat. Nanotechnol.*, 2012, **7**, 825–832.
4 H. P. Cong, P. Wang and S. H. Yu, *Chem. Mater.*, 2013, **25**, 3357–3362.
5 E. Koh, S.-Y. Baek, N.-K. Kim, S. Lee, J. Shin and Y.-W. Kim, *New J. Chem.*, 2014, **38**, 4409–4419.
6 S. R. White, N. R. Sottos, P. H. Geubelle, J. S. Moore, M. R. Kessler, S. R. Sriram, E. N. Brown and S. Viswanathan, *Nature*, 2001, **409**, 794–797.
7 X. X. Chen, M. A. Dam, K. Ono, A. Mal, H. B. Shen, S. R. Nutt, K. Sheran and F. Wudl, *Science*, 2002, **295**, 1698–1702.
8 B. Ghosh and M. W. Urban, *Science*, 2009, **323**, 1458–1460.
9 Y. Amamoto, J. Kamada, H. Otsuka, A. Takahara and K. Matyjaszewsk, *Angew. Chem., Int. Ed.*, 2011, **50**, 1660–1663.
10 M. Burnworth, L. Tang, J. R. Kumpfer, A. J. Duncan, F. L. Beyer, G. L. Fiore, S. J. Rowan and C. Weder, *Nature*, 2011, **472**, 334–337.
11 R. S. Trask and I. P. Bond, *Smart Mater. Struct.*, 2006, **15**, 704–710.
12 D. Y. Wu, S. Meure and D. Solomon, *Prog. Polym. Sci.*, 2008, **33**, 479–522.
13 L. Huang, N. Yi, Y. Wu, Y. Zhang, Q. Zhang, Y. Huang, Y. Ma and Y. Chen, *Adv. Mater.*, 2013, **25**, 2224–2228.
14 S. Neuser, V. Michaud and S. R. White, *Polymer*, 2012, **53**, 370–378.
15 G. Li, H. Meng and J. Hu, *J. R. Soc., Interface*, 2012, **9**, 3279–3287.
16 X. Luo and P. T. Mather, *ACS Macro Lett.*, 2013, **2**(2), 152–156.
17 B. T. Michal, C. A. Jaye, E. J. Spencer and S. J. Rowan, *ACS Macro Lett.*, 2013, **2**, 694–699.
18 X. Wang, J. Zhao, M. Chen, L. Ma, X. Zhao, Z. Dang and Z. Wang, *J. Phys. Chem. B*, 2013, **117**, 1467–1474.
19 S. Thakur and N. Karak, *J. Mater. Chem. A*, 2014, **2**, 14867–14875.
20 S. Thakur and N. Karak, *Carbon*, 2012, **50**, 5331–5339.
21 X. Zhao, Z. Zhang, L. Wang, K. Xi, Q. Cao, D. Wang, Y. Yang and Y. Du, *Sci. Rep.*, 2013, **3**, 3421.
22 M. Bernardi, M. Palummo and J. C. Grossman, *Nano Lett.*, 2013, **13**, 3664–3670.
23 Y. J. Chen, P. Gao, C. L. Zhu, R. X. Wang, L. J. Wang, M. S. Cao and X. Y. Fang, *J. Appl. Phys.*, 2009, **106**, 054303.
24 S. Thakur and N. Karak, *Prog. Org. Coat.*, 2013, **76**, 157–164.
25 S. Thakur and N. Karak, *Mater. Chem. Phys.*, 2014, **144**, 425–432.
26 S. Thakur and N. Karak, *RSC Adv.*, 2013, **3**, 9476–9482.
27 D. Cai, J. Jin, K. Yusoh, R. Rafiq and M. Song, *Compos. Sci. Technol.*, 2012, **6**, 702–707.
28 J. R. Potts, D. R. Dreyer, C. W. Bielawski and R. S. Ruoff, *Polymer*, 2011, **52**, 5–25.
29 X. Wang, Y. Hu, L. Song, H. Yang, W. Xing and H. Lu, *J. Mater. Chem.*, 2011, **21**, 4222–4427.
30 S. Thakur and N. Karak, *ACS Sustainable Chem. Eng.*, 2014, **2**, 1195–1202.
31 H. Kalita and N. Karak, *Polym. Bull.*, 2013, **70**(11), 2953–2965.
32 Y. Bai, Y. Chen, Q. Wang and T. Wang, *J. Mater. Chem. A*, 2014, **2**, 9169–9177.
33 R. M. Hodlur and M. K. Rabinal, *Compos. Sci. Technol.*, 2014, **90**, 160–165.
34 R. K. Layek, A. Kundu and A. K. Nandi, *Macromol. Mater. Eng.*, 2013, **298**, 1166–1175.
35 F. H. Jeong, J. Yang, H. S. Lee, S. W. Seo, D. H. Baik and J. Kim, *J. Appl. Polym. Sci.*, 2008, **107**, 803–809.

 